East Eur. J. Phys. Vol.1 No.3 (2014) 55-67

PACS: 28.41.Qb, 96.50.Vg, 78.70.-g, 32.80.Cy, 78.70.En, 81.05.-t, 81.05.Ni, 81.20.Vj, 02.70.-c, 02.70.Uu

MONTE CARLO EVALUATION OF THE RADIATION SHIELDING EFFICIENCY OF LAMINATED COMPOSITES UNDER ELECTRON AND PHOTON IRRADIATION

B.V. Borts[1], M.I. Bratchenko[1], S.V. Dyuldya[1], I.G. Marchenko[1,2], D.A. Sanzharevsky[1], V.I. Tkachenko[1,2]

[1] National Science Center "Kharkiv Institute of Physics and Technology"
Akademichna Str. 1, 61108, Kharkiv, Ukraine
[2] V.N. Karazin Kharkiv National University
Svobody Sq. 4, 61022, Kharkiv, Ukraine
E-mail: tkachenko@kipt.kharkov.ua
Received June 26, 2014

The heterogeneity effect on the shielding efficiency of laminated composites under electron and gamma irradiation of moderate (~MeV) energies was studied. The effect was quantified, by means of Monte Carlo method, in terms of the asymmetry of the bimetallic dual layer system's AlW shielding efficiency depending on the direction (Al–W *vs.* W–Al) of both electron and photon irradiation. The charged particles and bremsstrahlung radiation transport was simulated for electron irradiation of the 9-layer composite test sample fabricated by the vacuum hot rolling solid phase welding of Ti–Ni–Cu–Nb–Cu–$(W–Cu)_2$ layers. Dose and photon kerma rates behind the laminated shielding were calculated and the prospects of its application under severe constraints both on shielding weight and dimensions were substantiated.
KEYWORDS: electrons, photons, radiation shielding, laminated composite materials, Monte Carlo method.

ОЦІНЮВАННЯ МЕТОДОМ МОНТЕ-КАРЛО РАДІАЦІЙНО-ЗАХИСНОЇ ЕФЕКТИВНОСТІ ШАРУВАТИХ КОМПОЗИТІВ ПІД ОПРОМІНЕННЯМ ЕЛЕКТРОНАМИ І ФОТОНАМИ

Б.В. Борц[1], М.І. Братченко[1], С.В. Дюльдя[1], І.Г. Марченко[1,2], Д.А. Санжаревський[1], В.І. Ткаченко[1,2]

[1] Національний науковий центр «Харківський фізико-технічний інститут»
61108 Україна, м. Харків, вул. Академічна, 1
[2] Харківський національний університет імені В.Н. Каразіна
61022, Україна, м. Харків, пл. Свободи 4

Досліджений вплив гетерогенності шаруватих композитів на ефективність захисту ними від електронного та γ-опромінення помірних (~МеВ) енергій. Методом Монте-Карло він охарактеризований кількісно в термінах асиметрії захисних показників біметалічної двошарової системи AlW в залежності від напрямку (Al–W чи W–Al) опромінення обох видів. Для електронного опромінення експериментального зразка 9-шарового композита Ti–Ni–Cu–Nb–Cu–$(W–Cu)_2$, виготовленого з'єднанням шарів у твердій фазі шляхом гарячої прокатки в вакуумі, промодельований перенос у зразку зарядженої й гальмівної компонент випромінювання, розраховані потужності дози й фотонної керми за захисною структурою та обгрунтована перспективність її застосувань за жорстких обмежень одностайно за вагою та габаритами захисту.
КЛЮЧОВІ СЛОВА: електрони, фотони, радіаційний захист, шаруваті композитні матеріали, метод Монте-Карло.

ОЦЕНКА МЕТОДОМ МОНТЕ-КАРЛО РАДИАЦИОННО-ЗАЩИТНОЙ ЭФФЕКТИВНОСТИ СЛОИСТЫХ КОМПОЗИТОВ ПОД ОБЛУЧЕНИЕМ ЭЛЕКТРОНАМИ И ФОТОНАМИ

Б.В. Борц[1], М.И. Братченко[1], С.В. Дюльдя[1], И.Г. Марченко[1,2], Д.А. Санжаревский[1], В.И. Ткаченко[1,2]

[1] Национальный научный центр «Харьковский физико-технический институт»
61108, Украина, г. Харьков, ул. Академическая, 1
[2] Харьковский национальный университет им. В.Н. Каразина
61022, Украина, г. Харьков, пл. Свободы 4

Исследовано влияние гетерогенности слоистых композитов на эффективность защиты ими от электронного и γ-облучения умеренных (~МэВ) энергий. Методом Монте-Карло оно охарактеризовано количественно в терминах асимметрии защитных показателей биметаллической двухслойной системы AlW в зависимости от направления (Al–W или W–Al) облучения обоих видов. Для электронного облучения экспериментального образца 9-слойного композита Ti–Ni–Cu–Nb–Cu–$(W–Cu)_2$, изготовленного соединением слоёв в твёрдой фазе путём горячей прокатки в вакууме, промоделирован перенос в образце заряженной и тормозной компонент излучения, рассчитаны мощности дозы и фотонной кермы за защитной структурой и обоснована перспективность её применений при жестких ограничениях одновременно по весу и габаритам защиты.
КЛЮЧЕВЫЕ СЛОВА: электроны, фотоны, радиационная защита, слоистые композитные материалы, метод Монте-Карло.

R&D of materials for efficient protection against ionizing radiation [1,2] still remains an actual direction of radiation physics and engineering. Biological shielding of nuclear reactors, neutron sources and charged particles accelerators, tanks for spent nuclear fuel and radioactive waste, protective components of medical equipment and clothing [3] are common applications of shielding materials. Other applications of great fundamental value are the background minimization in low-background experiments on Dark Matter [4] and double β-decay searches, protection of radiation detectors [5] and electronics in nuclear medicine as well as on interplanetary spacecrafts and satellites of the Earth [6,7].

The general function of shielding materials is to reduce the rate of absorbed dose *D* [1,2,8] of radiation in the vital

parts of a system to an acceptable level compliant to working standards, or objectives and conditions of experiments. The shielding material optimum selection is then determined by the kind and energy spectrum of radiation. The optimization issues are often occasioned by an urgent need of simultaneous efficient protection against various kinds of radiation, *e.g.*, neutrons and γ-rays in nuclear reactors, electrons, protons, X- and γ-rays in space applications, and so on.

It is worth noting that such a diversity is not only due to multi-component nature of primary radiation sources but also emerges, in matter, from secondary processes at cascade development of electromagnetic (e.-m.) and nuclear interactions. Typical examples are γ-rays produced at inelastic interactions of neutrons with nuclei of reactor fuel, structural and shielding materials, bremsstrahlung of accelerated relativistic electrons as well as the electron-photon, muon and hadron showers at passage of high-energy cosmic rays through matter [4].

From the standpoint of end-user industrial applications, special attention, in the design of radiation shielding and the selection of appropriate materials, has to be paid to the minimization of weight and/or geometrical dimensions of shielding relevant component parts of different equipment and devices, as well as to the durability of their operation under extreme conditions of high temperature and mechanical stress. These requirements are usually considered as optimization criteria which are specific to each application.

A promising way of the complex radiation environments operating shielding optimization is the application of composite materials and, in particular, of laminated multi-layer structures and coatings. Just the heterogeneity of these structures improves their protective efficiency taking into account all the above-mentioned constraints peculiar to specific applications. For example, to protect against γ-rays used are the so called "graded-*Z*" laminated structures [3] having atomic numbers *Z* of layer materials successively decreasing from high-*Z* (Pb, W, Ta) to low-*Z* (Sn, Cu, Fe, Al) ones in the direction of radiation propagation. The main function of the sequence of low-*Z* layers is to absorb the secondary Auger electrons and fluorescent X-ray photons emitted at scattering and absorption of γ-rays in the preceding *Z*-ordered layers of higher-*Z* materials. Such a protective structure is frequently more lightweight than the single-layer heavy metal shielding. Laminated composites of materials of different *Z* were also proposed [6,7,9,10] for protection against protons and β-radiations (moderately relativistic electrons) especially relevant to a shielding of spacecrafts in Earth orbits [9,11]. In this case of charged particles irradiation, the due selection of the layers alternation promotes the suppression of the yield of secondary bremsstrahlung γ-quanta extremely undesirable in view of their high penetrability.

From the point of view of the materials science and technology, of great practical value is the perfecting of the laminated shielding composites fabrication methods. This is especially true in poor compatibility of the materials they should be composed of. One of these methods, the joint of layers of dissimilar materials in the solid phase by their vacuum hot rolling [12], is developed and practicing in NSC KIPT. It allows to obtain multilayer composite materials having high physical and mechanical properties. This makes the laminated composites thermal stress resistant and well-deformable to impart the specific applications' required shapes without the loss of layers integrity. The method is applicable to virtually arbitrary combinations of metals in the multilayer composite. However, the structural complexity of such laminates confronts the shielding design engineers with the task of reliable prediction of their radiation protection parameters which do not reduce to the well-known tabular data [1,2] for standard shielding materials.

The design and optimization of compositionally and structurally complex radiation shielding requires both the large amount of experimental tests carried out in conditions close to the expected radiation environments and the fine preliminary calculations of the efficiency of the developing material and/or structure with an accuracy comparable with that of experimental measurements. The application of computational technique to the design of heterogeneous shielding has a long history [1,9,13,14] and can significantly reduce the costs of finding of the most appropriate option and the amount of ionizing radiation sources involvement in the R&D procedures. Currently, the precise methods of computer modeling of radiation propagation through heterogeneous media are widely used for these purposes. Particularly, this is the Monte Carlo (MC) method [15]. It is implemented in numerous computer codes which offer the most adequate and comprehensive simulation of all elementary physical processes of interaction of ionizing radiations with materials and structures complex by their geometry as well as by their elemental and isotopic composition.

The present paper deals with the application of Monte Carlo simulation to the study of peculiarities of the passage of MeV-energy electrons, the accompanied bremsstrahlung, X-ray and γ-beams through dual and multilayer shielding structures. This advances the previous studies of the authors [16–18], and extends the use of simulation to the assessment of shielding efficiency of the sample of multilayer structure obtained by the solid phase welding of metals.

PROBLEM SETUP

The objective of this work is the detailed computational description of the spectral and dosimetric characteristics of radiation passed through certain typical examples of laminated shielding structures.

We restrict ourselves to the protection against electrons of moderately relativistic energies $E_e = 0.5 \div 3$ MeV as well as against photons of energies $E_\gamma = 10^1 \div 10^3$ keV in the X-ray and γ-range, the topical cases for many electro-physical irradiation processes, medical, and space applications. We shall consider different, by the layers' composition and alternation order, laminated shields under irradiation by broad parallel beams of electrons and photons.

Our task is to calculate the energy spectra of various kinds of the shielding emerged radiation along with the efficiency relevant and the dosimetry standards compliant physical quantities [1,2,8] such as the attenuation factor *k*, the photon air-kerma *K* and the dose *D* absorbed in a solid-state detector located immediately behind the shielding.

Two interrelated goals are pursued in this paper at the subsequent analysis of the results of calculations.

First, we investigate quantitatively the laminated shields' heterogeneity impact on their radiation-protective efficiency ratings. For model bimetallic dual layer system of tungsten and aluminum, this is done in terms of the asymmetry of these ratings depending on the order (Al–W *vs.* W–Al) of layers the relativistic electron or photon beams pass through the shield. We identify and discuss the essentially different nature of the asymmetry effect in these two cases.

Next, we proceed to the example of a real multilayer shielding composite TiNiNbWCu fabricated by the solid phase welding of different metals and designed for optimized protection against electrons with energies up to 3 MeV. The goal is to rate this laminated composite quantitatively for this specific use-case. The results of calculations of various dosimetric quantities are compared, as functions of electron energy, with the corresponding results for typical single-element materials widely used for protection against β– and γ-radiation. Basing on such a comparative analysis, we discuss possible applications of this novel composite material and the prospects of application of our computational technique to further R&D of composite shielding.

SIMULATON METHOD AND COMPUTER CODES

To simulate the (e^-,γ) transport in laminated shields, we use two completely independent general-purpose MC codes, the extensively validated commercial code PENELOPE [19,20] (we already used it earlier in refs. [17,18]) and the multi-purpose code RaT 3 [21] developed in-house in NSC KIPT on the basis of the open-source libraries GEANT4 OO Toolkit [22]. Both of these codes make use of the Monte Carlo method of the numerical modeling of the radiation interaction with matter. The method consists in the successive sampling of random events of the elementary processes of radiations interaction with atomic nuclei and electrons of the medium and the statistical estimation ("tallying") of the expected mean values of various physical quantities, including the dosimetric ones, to be measured in real experiments. Thus, these codes implement the computer experiment methodology [21] to simulate a natural one at a very limited use of model assumptions. This allows to predict and, in prospect, to optimize the parameters of the systems under design.

In our calculations, both of the applied codes took into account the complete systematics of the e.-m. processes of radiation particles interaction with media. These are: the electrons and positrons ionization and radiation stopping resulted in their slowing-down and emission of bremsstrahlung photons; the multiple nuclear scattering of charged particles and the production of high-energy δ-electrons; the photoabsorption which produces secondary electrons and fluorescent photons; the photons incoherent (Compton) and coherent (Rayleigh) scattering and their γ-conversion to $e^{\pm}$-pairs followed by emission of annihilation γ-quanta. Hadronic processes (such as photonuclear reactions) were omitted from calculations as irrelevant to the considered energy range of radiations.

The PENELOPE code is focused exclusively on the simulation of e.-m. processes of leptons and photons interaction with matter in a wide ($\sim 10^1 \div 10^9$ eV) range of energies. In this area, the code manifests an outstanding accuracy of physical models, data and algorithms [20]. This allows to rate it as a reference code. On the other hand, the research code RaT 3 inherits all the variety of physical models and data banks of GEANT4 package [22] which cover the physics of elementary particles as well as the high-energy hadron, and neutron physics. Therefore, it has a much wider range of applications [21]. RaT 3 fully incorporates various options of physical models of the above-listed e.-m. interaction processes. Moreover, modern versions of GEANT4 contain a set of e.-m. models which is specifically focused on the reproduction ('emulation') of the physics of the standard code PENELOPE. We mainly used this subset of GEANT4 models for the RaT code based simulations. It is worth noting here that the extra task of this paper, the methodical one, was the comparison of the modeling results obtained using both options of the applied software, PENELOPE and RaT.

ASYMMETRY OF THE PROTECTIVE EFFICIENCY OF BIMETALLIC COMPOSITES

Aluminum with density $\rho_{Al} = 2.7$ g/cm^3, and the $\rho_W = 19.3$ g/cm^3 dense tungsten were chosen as the conventional shielding materials for protection against different kinds of radiation which we consider in this paper. Aluminum is widely used for protection against electron flows of moderate energies (particularly, in aerospace engineering having in mind its low specific gravity). However, it is a lightweight material which is ineffective for protection against γ-radiation due to its small $Z = 13$ (and, hence, a low concentration of electrons), and low density. The heavy tungsten ($Z = 74$) is preferable with respect to both of these parameters, and is widely used in X-ray and γ-radiation shielding. However, under irradiation by relativistic electrons of energies we consider here, the use of tungsten as a shielding material is impractical since, despite of the relatively small ranges $R_W \sim 1$ cm of such electrons in W, tungsten is one of the most efficient converters of their energy into bremsstrahlung. This virtually annuls all the protective effect.

We will study the protective properties of a laminate of these materials depending on which side it is irradiated by electrons or photons. So, we consider two systems having the low-Z (Al–W) or the high-Z (W–Al) metal at front.

Electron irradiation

Let's first compare the spectral properties of radiations observed behind the equally thick plates of each of the considered materials the bimetallic composite is made of.

The PENELOPE code calculated energy spectra $f(E)$ of electrons of initial energy $E_e = 2$ MeV after the passage

through $t_{Al} = t_W = 1$ mm thick slabs of aluminum and tungsten are shown in Fig. 1(a). Obviously, they are different qualitatively, as well as differ quantitatively by several orders of magnitude.

Such a behavior of MC simulated spectra of Fig. 1(a) is quite explainable and agrees well with simple estimations.

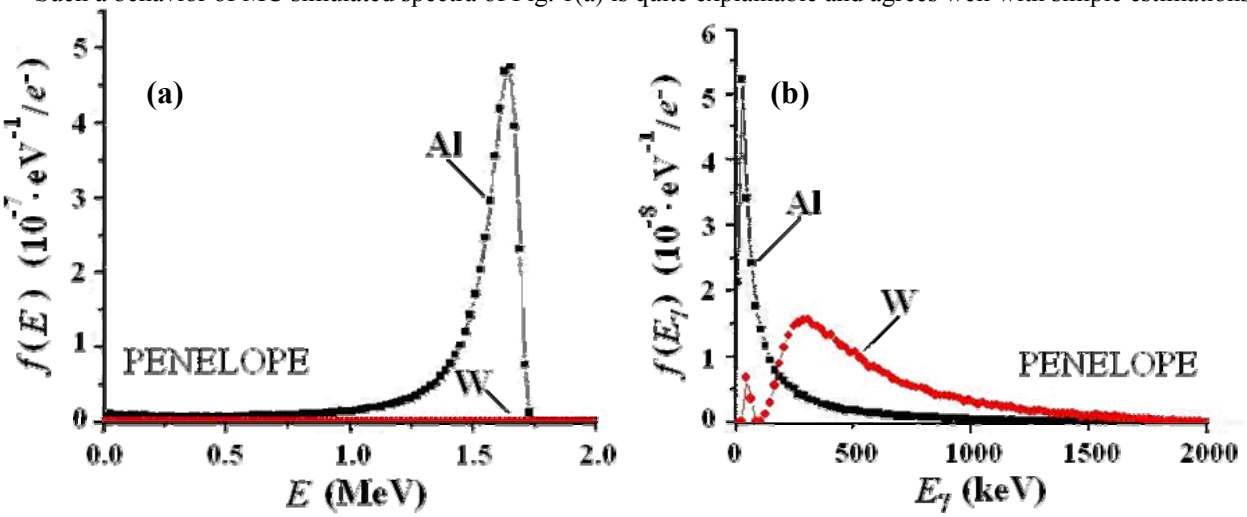

Fig. 1. Energy spectra of electrons (a) and photons (b) behind the 1 mm thick slabs of aluminum (Al) and tungsten (W) calculated for electron beam initial energy $E_e = 2$ MeV. Monte Carlo simulation by means of the PENELOPE code.

According to the U.S. NIST standard calculator ESTAR [23], the CSDA range R_{Al} of 2 MeV electrons in aluminum equals to 1.224 g/cm^2 = 4.53 mm > t_{Al} = 1 mm. Therefore, the 1 mm thick aluminum plate lets through a significant (~70%) fraction of primary electrons having the well shaped energy spectrum. At the same incident beam energy, the same ESTAR code reports the total specific stopping power $S = \rho^{-1} \cdot |dE/dz|$ of Aluminum $S_{Al} = 1.518$ MeV·cm^2/g which results in the mean energy loss rate $|dE/dz| = \rho_{Al} \cdot S_{Al} = 410$ keV/mm. This explains the pronounced spectral peak of Fig. 1(a) at $E \approx 1.6$ MeV $\approx$ 2 MeV – 410 keV/mm × 1 mm. The finite peak width is mainly due to the energy loss fluctuations taken into account by the simulation code. The low-energy spectral tail is the result of the electrons path length fluctuations due to multiple scattering by target atoms.

In tungsten, the range R_W(2 MeV) = 1.613 g/cm^2 = 0.8 mm < t_W = 1 mm. Therefore, the primary beam electrons are almost completely absorbed in the tungsten slab of chosen thickness. At first glance, this manifests its good protective ability. However, this conclusion is wrong if we recall the secondary bremsstrahlung produced by electrons. In Fig. 1(b), shown are the PENELOPE code calculated energy spectra $f(E_\gamma)$ of photons behind the same slabs of Al and W. By photon energy E_γ, they spread from X-ray energy range (<100 keV) up to the initial energy of electrons.

In a low-Z Aluminum, photoabsorption is unsubstantial down to very low photon energies $E_\gamma < 30$ keV [24]. Thus, the $f(E_\gamma)$ shape agrees well with the known shape ($\propto 1/E_\gamma$) of the Shiff bremsstrahlung spectrum. For high-Z and dense tungsten, the strong self-absorption of bremsstrahlung photons occurs in a target. This violates the Shiff spectral dependency below $E_\gamma < 0.5$ MeV, and results in a relatively broad spectral maximum near $E_\gamma \approx 300$ keV. Besides, the sharp low-energy peak of fluorescent X-ray photons is observed at energies in the vicinity of the Tungsten K_α и K_β series (≈60÷70 keV). These secondary X-rays emerge from the thin surface layer at the rear edge of the tungsten slab.

As concerns the radiation-shielding properties of materials, Fig. 1(b) clearly shows that the spectral density of high-energy ($E_\gamma > 0.2$ MeV) highly penetrable bremsstrahlung γ-quanta is significantly higher for the tungsten shield as against that of the shield of lightweight aluminum. With respect to this parameter, tungsten acts as a converter rather than the shielding material.

Now let's proceed to the sandwich structures Al–W and W–Al which correspond to the heterogeneous bimetallic composite of the same slabs having total thickness $t = t_{Al} + t_W$ =2 mm and irradiated, from different sides, by 2 MeV electrons. The data of Fig. 1(a) clearly show that both sandwiches guarantee an excellent protection against the primary beam electrons since 1 mm thick layer of tungsten is common to both of the structures. Therefore, it is sufficient to compare them with respect to the intensity parameters of the produced secondary bremsstrahlung.

Energy spectra of photons emerged from Al–W and W–Al targets are shown in Fig. 2. In this figure, the simulation data of the PENELOPE code (markers, we obtained these data earlier in ref. [18]) are supplemented with the results of the RaT code simulation (histograms). We note the good quantitative agreement of the simulation results of both codes throughout the whole range of photon energies. This also confirms the possibility to focus hereinafter on the outputs of the RaT code which is more flexible in respect of the problem setups and deep analysis of the modeling results.

By shape, the Fig. 2 spectra are similar to each other as well as to the Fig. 1(b) spectrum of photon emission from the tungsten plate. However, about 1.5÷2 times high asymmetry of Al–W and W–Al systems is found with respect to the spectral density values in the whole range of the bremsstrahlung energies. The same order of magnitude quantifies

the asymmetry of the spectral energy distributions $F(E_\gamma) = E_\gamma f(E_\gamma)$ of emitted photons as well as that of the integral dosimetric functionals like $\propto \int \mu_{en}(E_\gamma)\cdot F(E_\gamma)\mathrm{d}E_\gamma$ with photon-to-medium energy transfer coefficient $\mu_{en}(E_\gamma)$. With respect to all these parameters, the system Al–W looks more preferable, as a shielding structure, than the W–Al system.

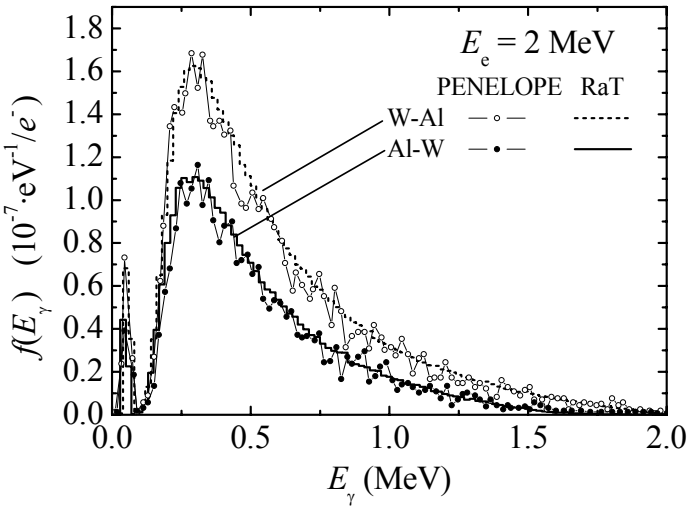

Fig. 2. Energy spectra of photons behind the 2 mm thick dual layer laminated composite of 1 mm thick plates of tungsten and aluminum depending on the order of W and Al layers the 2 MeV electrons pass through. Simulation by means of the PENELOPE (markers) and RaT 3 (histograms) Monte Carlo codes.

The main physical reason of the effect consists in the well-known correlation of ionization ($|\mathrm{d}E/\mathrm{d}z|_{ion} \propto Z/A$) and radiative ($|\mathrm{d}E/\mathrm{d}z|_{rad} \propto Z^2/A$) energy loss rates of relativistic electrons in a material having an atomic number Z and atomic mass A. The ratio $r = |\mathrm{d}E/\mathrm{d}z|_{rad} / |\mathrm{d}E/\mathrm{d}z|_{ion} \propto Z$ grows approximately linearly with the increase of an atomic number of a material. For Tungsten, it is substantially greater ($r_W/r_{Al} \approx 5.7$) than for Aluminum.

This suggests a simple qualitative explanation of the observed effect of asymmetry. Since the ranges of secondary δ-electrons are too small for their noticeable escape from the shield, the role of ionization stopping $|\mathrm{d}E/\mathrm{d}z|_{ion}$ reduces only to a slowing down of the e^--beam particles which pass through a material. From the other hand, radiative stopping $|\mathrm{d}E/\mathrm{d}z|_{rad}$ transforms the energy of electrons into that of highly penetrating secondary bremsstrahlung. For both of Al–W and W–Al systems, principal production of bremsstrahlung occurs inside the layer of tungsten. For the W–Al system, bremsstrahlung is only slightly attenuated in the successive aluminum layer where its local production rate is significantly weaker (see Fig. 1(b)). In the Al–W structure, the tungsten layer is effectively irradiated by electrons having the noticeably smaller energies (~1.6 MeV and less, see Fig. 1(a)) than the incident beam energy, 2 MeV. Radiative energy loss rate of electrons decreases approximately linearly with the decrease of their energy. Therefore, the production rate of γ-quanta in a tungsten layer decreases, as it is clearly evidenced by the data of Fig. 2.

Photon irradiation

Let's proceed to the case of Al–W and W–Al systems irradiation by photons of different energies E_γ.

For this case, we adopted the layers thicknesses $t_{Al} = 0.25$ cm and $t_W = 0.25$ mm since the shielding properties of such a sandwich were experimentally studied in NSC KIPT [16]. We shall also compare certain results of simulation of such a "thin" laminate with those we obtain for its tenfold scaled version, the "thick" system having $t_{Al} = 2.5$ cm and $t_W = 0.25$ cm. As of their mass per unit front surface area, these laminated composites are equivalent to the slabs of an effectively homogenized alloy $Al_{58.3}W_{41.7}$ (%wt) having a density $\rho_{eff} = 4.21$ g/cm^3 and the thicknesses $t_{eff} = 2.75$ mm and 2.75 cm, respectively for "thin" and "thick" options.

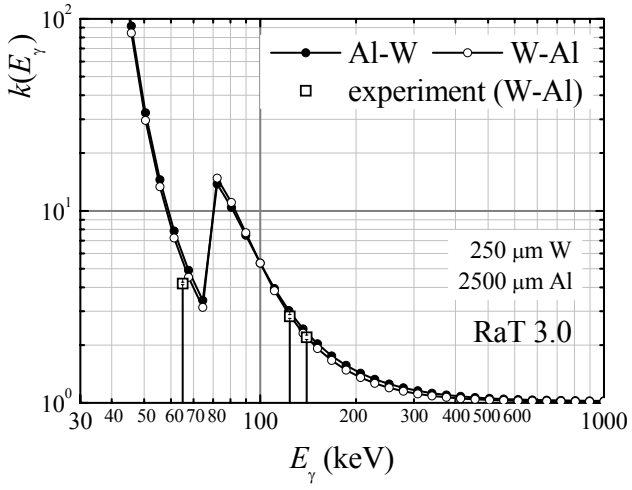

Fig. 3. Energy dependencies of attenuation factors $k(E_\gamma)$ at passage of photons with different energies E_γ through dual layer bimetallic laminated composites Al–W (●) and W–Al (○)in comparison with experimental data [16] for the system W–Al (□).

The natural measure of the photon irradiation relevant shielding efficiency is the attenuation factor k. It is defined [1,2] as the ratio of the values of any (but the same) dosimetric functionals [8] of the photon flux ϕ (*e.g.*, the energy flux Φ, exposure X or air-kerma K) just before, and behind shielding. For definiteness, below we calculate the attenuation factor $k(E_\gamma)$ of the energy flux $\Phi(E_\gamma) = E_\gamma \times \phi(E_\gamma)$ of monochromatic photons. In these terms, $k(E_\gamma) = \Phi_0(E_\gamma) / \Phi(E_\gamma)$ where zero subscripts the primary energy flux.

The RaT code calculated $k(E_\gamma)$ of "thin" bimetallic composites Al–W and W–Al are shown in Fig. 3 for a wide range of photon energies E_γ. The data calculated for the homogenized alloy $Al_{58.3}W_{41.7}$ lie between the curves for Al–W and W–Al systems.

This figure also presents the W–Al sandwich attenuation factor measurements results [16]. They are well described by simulation for the cases of spectral lines ^{57}Co (122 and 136.5 keV). A little bit worse agreement is found for the 59.5 keV line of Americium ^{241}Am.

This is probably due to ~10% variance (which was omitted in our model) of the thickness of the foils used for measurements. In general, the agreement of simulation and experimental data is quite satisfactory.

As expected, the attenuation factors of Fig. 3 generally increase with decreasing of E_γ but manifest a resonant behavior near the energies of the absorption edges of Tungsten. For our simulation statistics, ~10^8 histories of primary photons per each E_γ, the Monte Carlo estimation r.m.s. statistical error is smaller than the size of the Fig. 3 markers. Therefore, their exists the statistically valid difference of attenuation factors $k^{(\text{Al–W})}(E_\gamma)$ and $k^{(\text{W–Al})}(E_\gamma)$ for all E_γ. Note that mostly $k^{(\text{Al–W})}(E_\gamma) > k^{(\text{W–Al})}(E_\gamma)$. Thus, similar to the above considered case of electron irradiation, the asymmetry of shielding efficiency takes place. As a whole, the "light–to–heavy" combination is preferable.

To quantify the observed effect, let's introduce the asymmetry factor $\eta(E_\gamma) = k^{(\text{Al–W})}(E_\gamma) / k^{(\text{W–Al})}(E_\gamma)$. Its energy dependence is shown in Fig. 4(a) and is supplemented, in Fig. 4(b), with the results obtained at the simulation of the scaled "thick" system. Besides, these plots' open markers indicate the ratio $\eta_{\text{eff}}(E_\gamma) = k^{(\text{Al–W})}(E_\gamma, t = t_{\text{Al}}+t_{\text{W}}) / k^{(\text{eff})}(E_\gamma, t_{\text{eff}})$ where $k^{(\text{eff})}$ is the attenuation factor of the t_{eff} thick mass-equivalent slab of effectively homogenized alloy $\text{Al}_{58.3}\text{W}_{41.7}$.

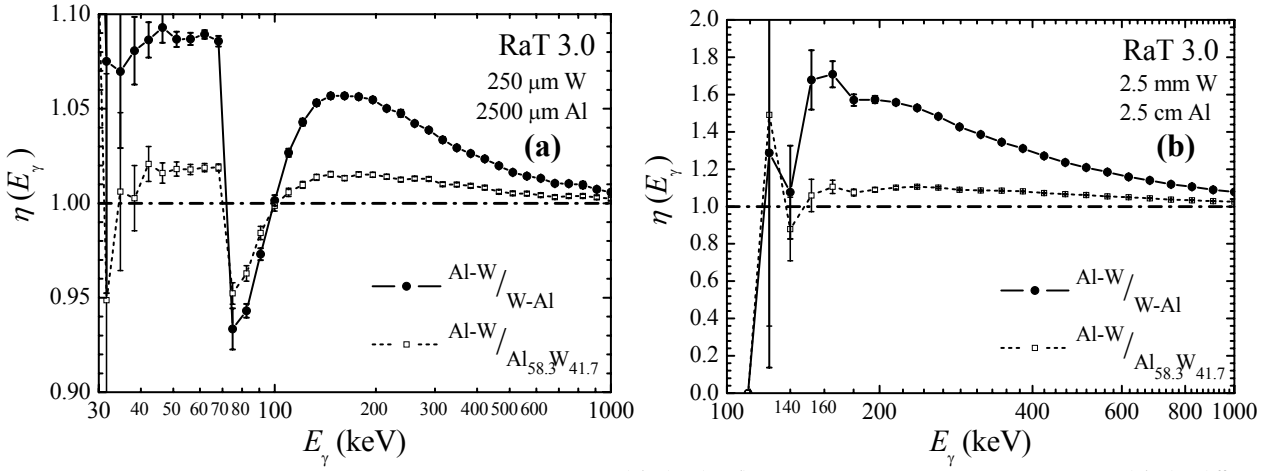

Fig. 4. Photon energy dependencies of the asymmetry factor $\eta = k^{(\text{Al–W})} / k^{(\text{W–Al})}$ (●) and the heterogeneity ratio $\eta_{\text{eff}} = k^{(\text{Al–W})} / k^{(\text{eff})}$ (□) for monochromatic photons attenuation by "thin" (a) and "thick" (b) dual layer bimetallic composites of aluminum and tungsten.

The data of Fig. 4 reveal several important patterns.

First, $\eta_{\text{eff}}(E_\gamma) \neq 1$. The heterogeneous and homogenized systems data divergence indicates the significant impact of the shielding layered heterogeneity on the attenuation of photons. It is also clear that the curves for multilayer systems $(\text{Al–W})_n$ shall lie between those of the dual layer and the homogenized systems tending to the latter one when $n \to \infty$.

Secondly, $\eta(E_\gamma)$ increases with the increase of the laminated shielding total thickness t. The asymmetry is relatively small, less than 10%, in the "thin" system (the experimental measurements [16] gave a rough estimate of the effect of ~5% at $E_\gamma < 100$ keV). In the "thick" system, the effect is grown in magnitude to about 70% at $E_\gamma \approx 160$ keV.

Finally, $\eta(E_\gamma) < 1$ for the "thin" system in the upper vicinity $E_\gamma \approx 75 \div 100$ keV of the photoabsorption K-edges of Tungsten. The W–Al system is more efficient there with respect to its protective properties.

All these features cannot own to the attenuation of an uncollided energy flux of primary photons. It obeys [1,2,8] the exponential Beer's law $\Phi^{(\text{prim})}(E_\gamma, t) = \Phi_0(E_\gamma) \cdot \exp[-\mu(E_\gamma) \cdot t]$ where t is a uniform slab thickness, $\mu(E_\gamma) = \lambda^{-1}(E_\gamma)$, cm^{-1}, is the linear attenuation coefficient of its material (the $\mu(E_\gamma)/\rho$ data for various media can be found, *e.g.*, in ref. [24]), $\lambda(E_\gamma)$ is the photon's mean free path length (MFP). Since the attenuation factor $k^{(\text{prim})}(t) = \Phi_0/\Phi^{(\text{prim})}(t) = e^{\mu t} = e^{t/\lambda}$ at each E_γ, the attenuation factor of a laminated composite having $\mu_i \neq \mu_j$, $(i \neq j)$ in each i^{th} of n layers of thickness t_i is

$$k_n^{(\text{prim})}\left(\sum_{i=1}^n t_i\right) = \exp\left(\sum_{i=1}^n \mu_i \cdot t_i\right) = \prod_{i=1}^n e^{\mu_i \cdot t_i} = \prod_{i=1}^n k_i^{(\text{prim})}(t_i).$$

As a product, it is the layers alternation order independent.

Therefore, the asymmetry is absent to the 1st order of the number of photons interaction events in the laminated shielding. It can be explained only taking into account the secondary effects of photons scattering and production of secondary radiations. The common practice of shielding calculations [1–3] treats these effects phenomenologically by the introduction of the so called buildup factors $B[\mu(E_\gamma) \cdot t] > 1$ which are pre-calculated, for a set of conventional shielding materials, in such a way that $\Phi(E_\gamma, t) = \Phi^{(\text{prim})}(E_\gamma, t) \times B[\mu(E_\gamma) \cdot t]$ in a homogeneous shield. Then, for our dual layer system, the asymmetry $\eta = k^{(\text{Al–W})} / k^{(\text{W–Al})} = B^{(\text{W–Al})}) / B^{(\text{Al–W})} \neq 1$ arises if $B^{(\text{W–Al})} \neq B^{(\text{Al–W})}$. Besides, it can be due to some other effects of photon scattering and re-emission such as, *e.g.*, their backscattering from the front surface of a shield.

These considerations are confirmed in our modeling. The RaT code calculated energy dependencies of the buildup factor $B(E_\gamma)$ and energy albedo $R_{\text{E}}(E_\gamma)$ for bi-directional photon irradiation of the "thin" system Al–W are plotted in Figure 5(a,b). Though all curves are qualitatively similar, the substantial quantitative differences both of $B(E_\gamma)$ and $R_{\text{E}}(E_\gamma)$ are evident for the cases of Al–W and W–Al systems. They can be immediately confronted with the asymmetry

observed in Fig. 4.

Secondary effects are noticeable ($B > 1$) already in a "thin" laminate. They are much more significant in a scaled "thick" system having attenuation factors $k \sim 10^5$ and the layer thicknesses t_{Al} and t_W which substantially exceed the MFPs $\lambda(E_\gamma)$ for all photon energies E_γ under consideration. This explains the much greater values of the asymmetry factors $\eta(E_\gamma)$ clearly seen in Fig. 4(b).

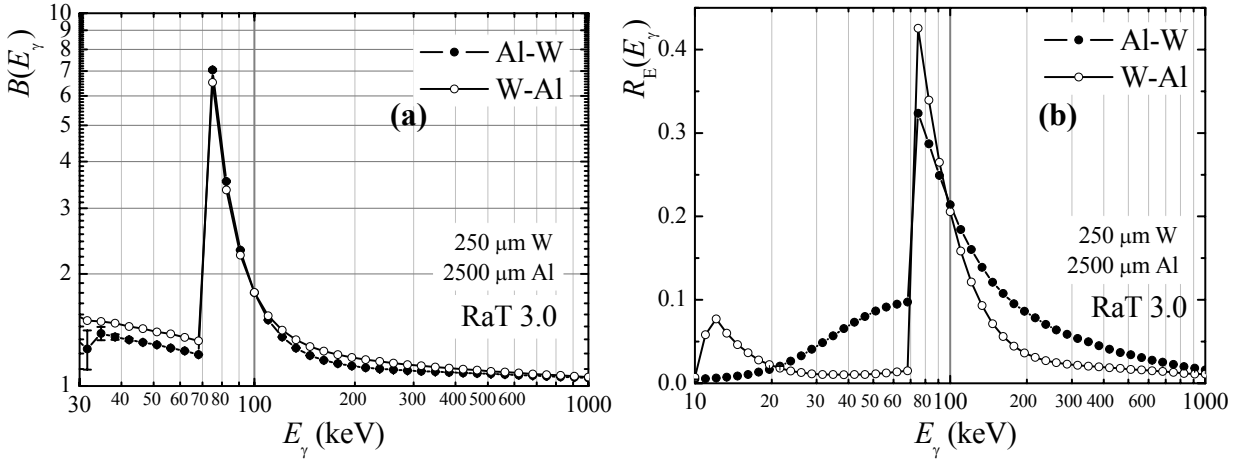

Fig. 5. Energy E_γ dependencies of buildup factors $B(E_\gamma)$ (a) and energy albedo $R_E(E_\gamma)$ (b) for photon irradiated dual layer bimetallic composites Al–W (○) и W–Al (●).

Correlating the Figs. 4(a) and 5(b) data quantitatively, we also found that $\eta(E_\gamma) \approx \left(1 - R_E^{(W-Al)}(E_\gamma)\right) / \left(1 - R_E^{(Al-W)}(E_\gamma)\right)$ for γ-quanta of sufficiently high $E_\gamma >> 10^2$ keV in a "thin" system. No such a correlation is observed for the "thick" system of Fig. 4(b) up to $E_\gamma = 1$ MeV. This is easy to explain if we introduce the reflectance $R \equiv R_E(E_\gamma)$, the transmittance $T(E_\gamma)$, and the shielding absorbed fraction $A(E_\gamma)$ of radiation energy flux in such a way that $R + A + T = 1$. Since, by definition, $k = T^{-1} = (1 - R - A)^{-1} \equiv (1 - R)^{-1} \times [(1 - R)/(1 - R - A)] \equiv (1 - R)^{-1} \times [(T + A)/T] \equiv (1 - R)^{-1} \times (1 + A/T)$, the necessary and sufficient condition of the observed correlation consists in the smallness $A/T << 1$ of the share A of absorbed radiation as against T, that of radiation passed through the shield. This is satisfied only in rather thin systems having $t \sim \lambda(E_\gamma)$ and $k(E_\gamma) \sim 1$, the case of our "thin" structure. In this case, the asymmetry effect is mainly due to the enhanced reflectance of the Al–W system. The "asymmetry–albedo" correlation is broken either at sufficiently low E_γ or in thick ($t >> \lambda(E_\gamma)$, $k(E_\gamma) >> 1$) shields. In such cases, $A/T >> 1$ and the asymmetry is mainly due to the difference in absorption.

In Fig. 5, the attention should be drawn to the abnormally high values of buildup and backscattering factors in the vicinity of the *K*-series photoabsorption edges of Tungsten just above the $K_{\beta 2}$ line energy, 69.088 keV. The anomaly of energy albedo is also well traced at E_γ above the *L*-series edges energies, 8÷12 keV. It is very probable that this determines the anomalous behavior of the asymmetry factors $\eta(E_\gamma)$ of Fig. 4(a) in the correspondent range of photon energies.

To clarify these fine details of the asymmetry effect foundation, we calculated, by means of the RaT code, the energy spectra of the photon energy flux behind "thin" Al–W и W–Al laminates for two photon energies, $E_\gamma = 220$ keV and 75 keV, which lie far from, and in the upper vicinity of the photoabsorption edge, respectively. The results are presented in Fig. 6(a,b). Smaller values of the spectral density, *esp.* in a high-energy range $E_{out} \sim E_\gamma$ which mainly contributes to the transmitted photons energy flux $\Phi(E_\gamma)$, correspond to better protective properties of the laminated shielding.

To understand the Fig. 6(a) spectra, one should note that the cross-section of incoherent Compton scattering exceeds the photoabsorption cross-section above $E_\gamma \approx 50$ keV in Al while only above $E_\gamma \approx 500$ keV in W [24]. This means that Aluminum is predominantly the Compton scatterer while Tungsten is mainly an absorber of 220 keV photons.

At energies E_{out} far above the *K*-edge of Tungsten, the Fig. 6(a) W–Al system relevant spectrum manifests the distinctive features of the Compton scattering of those photons which had not been absorbed in the tungsten layer. Indeed, according to the Compton effect kinematics, the final energy E' of a E_γ energy primary photon single scattered at an angle θ is $E'(E_\gamma, \theta) = E_\gamma \cdot m_e c^2 / \{E_\gamma \cdot (1 - \cos\theta)] + m_e c^2\}$ where $m_e c^2 = 511$ keV is the rest energy of electron. The energy E' is minimal at sideways scattering, $\theta = \pi/2$. In our case, $E'(220 \text{ keV}, \pi/2) = E_{min} \approx 154$ keV.

Both spectral densities of Fig. 6(a) leap down at the scattered photon energy $E_{out} = E_{min}$. However, the single scattering peak at $E_{out} \approx 160$ keV $> E_{min}$ is observed only for the W–Al system. It is absent in the spectrum of the Al–W system where scattered photons are efficiently absorbed in tungsten. At $E_{out} \approx 100$ keV, the broader peak of double Compton scattering is seen in the W–Al spectrum. This peak is also lost in the Al–W system where multiply scattered photons, along with their enhanced absorption in W, can scatter back from Al and contribute to the Fig. 5(b) albedo. At $E_{out} > 70$ keV, all these effects make the transmitted photons spectral density lower for the Al–W system. In Fig. 4(a),

this results in the asymmetry factors $\eta(E_\gamma) > 1$ at sufficiently high E_γ.

In the low-energy part, the Fig. 6(a) spectra are complicated because of secondary fluorescence of Tungsten. This has an opposite effect on the shielding transmittance asymmetry, and is illustrated in detail in Fig. 6(b).

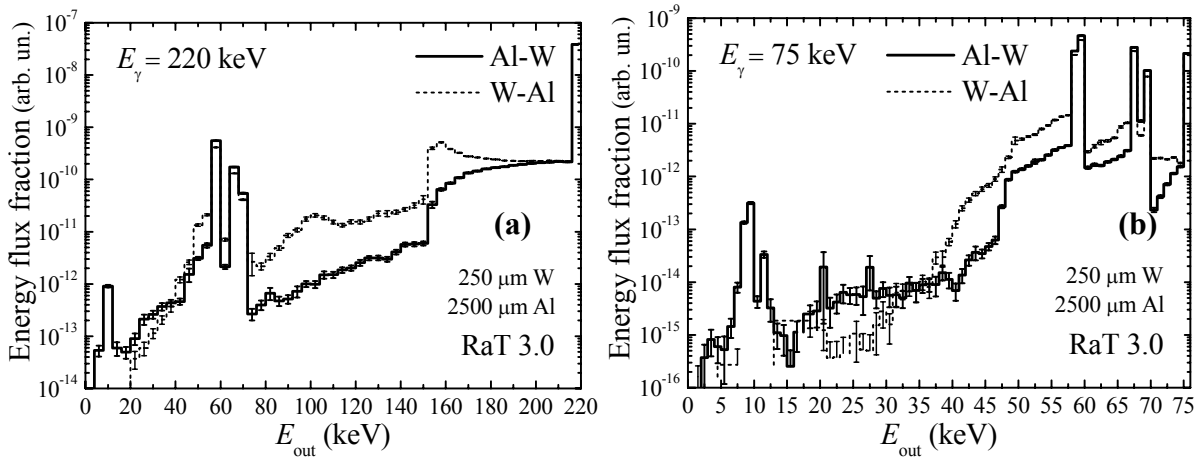

Fig. 6. Spectral distribution of the energy flux of photons of different energies E_{out} behind the laminated composites Al–W (bold curves) and W–Al (dashed curves) irradiated by monochromatic photons of energies E_γ = 220 keV (a) and 75 keV (b).

For E_γ = 75 keV, even the small-angle ($\theta << 1$) Compton scattering of primary photons can shift their energy by 6÷8 keV down to the energies of Tungsten *K*-series photoabsorption edges. Resonantly absorbed, these scattered photons induce the emission of fluorescent radiation having a discrete energy spectrum. The peaks in the high-energy part of Fig. 6(b) (also traceable in the low-energy part of Fig. 6(a) as a result of multiple Compton scattering of 220 keV primaries) correspond to different spectral lines of this X-ray response of the high-*Z* layer. The peak channel energies E_{out} agree well with those of W-$K_{\beta 1}$ (69.088 keV) and W-$K_{\beta 2}$ (67.248 keV) spectral lines as well as those of K_α-series (≈58÷59 keV) for the strongest peaks. The ~$10^{2\div 3}$ times weaker fluorescent response of the Tungsten *L*-series is also well resolved in the low-energy part E_{out} = 8÷12 keV of the emission spectrum.

Of key importance is that the X-ray yield of "thin" dual layer laminate is higher for Al–W system in all spectral peaks of Fig. 6(b). This is because of two reasons. First, the tungsten layer's effective thickness in the Al–W system becomes greater than the geometrical thickness t_W for photons Compton scattered in the preceding aluminum layer. This enhances the photoabsorption yield in tungsten. Secondly, some part of fluorescent photons emerged from the preceding tungsten layer of the W–Al system is absorbed in the successive layer of aluminum. Added in phase, both these effects result in the Fig. 4(a) asymmetry factor $\eta(E_\gamma) < 1$ just above the Tungsten photoabsorption edge energy.

Besides, the high flux of fluorescent X-ray photons explains the anomalously high values of the buildup factor $B(E_\gamma)$ in this range of energies (see Fig. 5(a)) while the abnormally high energy albedo $R_E(E_\gamma)$ of Fig. 5(b) is predetermined, in this energy region, by their practically isotropic angular distribution.

Discussion

The observed asymmetry effect justifies that the selection of a suitable alternation of layers of light and heavy materials can improve the efficiency of protection against both the electron and the photon irradiation. In both cases, the heterogeneity of the laminated composite affects only the characteristics of scattered and secondary radiations. Our calculations suggested that the "low-to-high-*Z*" sequence with increasing atomic number of the material is generally preferred in respect of the minimization of their production yield. However, this preference is of the essentially different physical reasons for these two cases of charged and neutral particles irradiation.

For electron irradiation, the "low-to-high-*Z*" sequencing allows suppression of the parasitic bremsstrahlung in the high-*Z* material by reason of the prior ionization slowing-down of the e^--beam in the layer of low-*Z* material which mainly plays a role of a beam energy damper. Obviously, this scenario is not something new since Al–W or Al–Pb composites are used for this reason, and for decades, in space, *e.g.*, in the design of manned spacecrafts [9]. In our simulation, the prevailed role of electrons stopping over that of their scattering is confirmed by the similarity of the shapes of bremsstrahlung spectra from Al–W and W–Al systems (see Fig. 2) which differ only by the photons yield magnitude.

The photon irradiation scenario is much less straightforward. On the one hand, the most dangerous high-energy γ-quanta are better absorbed in the "low-to-high-*Z*" structure by reason of the enhanced photoabsorption, in a high-Z layer, of those photons which have been heretofore Compton scattered in the low-*Z* layer material. This also promotes their enhanced backscattering off the shield. However, the inverse "high-to-low-*Z*" grading is more suitable for protection against X-rays because of suppression of resonance re-emission of fluorescent photons.

The natural idea [7,10] to combine the benefits of these two options can be embodied into the innovative designs of multilayer ($n > 2$) laminated composite shielding. One of such designs is considered below in the present paper.

ASSESSMENT OF THE RADIATION PROTECTION EFFICIENCY OF THE ATOMIC NUMBER PROFILED MULTILAYER COMPOSITE

The system under simulation consists of nine single-element metal layers positioned, in the direction of radiation propagation, in the following order:

$$\mathrm{Ti}^{Z=22}_{0.2\,\mathrm{mm}} \to \mathrm{Ni}^{Z=28}_{0.1\,\mathrm{mm}} \to \mathrm{Cu}^{Z=29}_{0.1\,\mathrm{mm}} \to \mathrm{Nb}^{Z=41}_{0.2\,\mathrm{mm}} \to \mathrm{Cu}^{Z=29}_{0.1\,\mathrm{mm}} \to \mathrm{W}^{Z=74}_{0.3\,\mathrm{mm}} \to \mathrm{Cu}^{Z=29}_{0.1\,\mathrm{mm}} \to \mathrm{W}^{Z=74}_{0.3\,\mathrm{mm}} \to \mathrm{Cu}^{Z=29}_{0.1\,\mathrm{mm}}.$$

Here superscripts denote the atomic numbers of the materials of layers while subscripts are their thicknesses.

At first, the layer material atomic number increases monotonically. Then this is followed by the alternating layers of heavier (Nb,W) and lighter (Cu) materials. The whole structure is an implementation of the "low-to-high-Z" option. It is similar to the Al–W system of the previous section with the peculiarity that the heavy metal layers alternate with thin (0.1 mm) layers of lighter copper. The functionality of these copper layers is of two kinds. First, they promote better adhesion at the metal interfaces and thereby improve the mechanical properties of the composite. Secondly, these local "high-to-low-Z" substructures act as scatterers and absorbers of fluorescent X-rays and secondary electrons from the heavy layers. Obviously, the main role plays the last copper layer located behind a thicker (0.3 mm) layer of tungsten.

The mass thickness $\rho{\cdot}t$ of the shielding structure was chosen to be equal to the CSDA range of 3 MeV electrons in Aluminum, $R_{\mathrm{Al}}(3\ \mathrm{MeV}) = 1.868\ \mathrm{g/cm^2}$ according to the ESTAR code calculation. This corresponds to the total thickness $t = 1.5$ mm of the laminated composite and to the thickness $t_{\mathrm{Al}} = 6.927\ \mathrm{mm} = 4.614{\cdot}t$ of the mass-equivalent aluminum slab.

The objective of this section is to describe the passage of relativistic electrons with energies E_e up to 3 MeV through this multilayer structure by means of the MC simulation and to evaluate, in such a way, its shielding efficiency.

The RaT code calculated depth z profiles of the radiation energy absorption rate are depicted with open markers in Fig. 7(a) for incident energies $E_e = 1$, 2, and 3 MeV. The solid curve indicates the PENELOPE code simulation data for $E_e = 2$ MeV. They agree well with those of RaT modeling. All these data describe the beam energy absorption integrally considering both the stopping of primary electrons and the attenuation of the produced bremsstrahlung γ-quanta. The energy loss rate slowdown by the end of the target qualifies it as a perfect electron absorber of a reasonably chosen thickness. Jumps at the boundaries of layers are due to different electron stopping powers and photon energy absorption coefficients of their materials. These jumps are especially great in the vicinity of Cu–W–Cu interfaces.

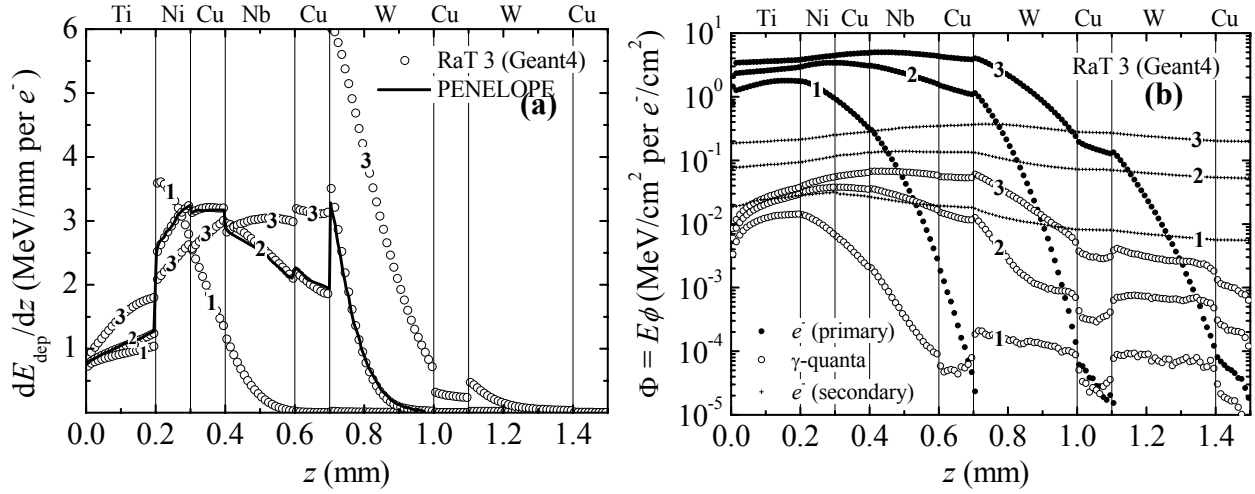

Fig. 7. The depth z dependencies of the electron beam energy absorption rate $|dE_{dep}/dz|$ (a) and energy fluxes Φ of primary and secondary electrons and bremsstrahlung γ-quanta (b) inside a laminated composite shielding TiNiNbWCu. The overlaying numbers on curves denote the electron beam incident energy E_e in megaelectronvolts. The results of calculations by means of the RaT 3 (markers) and PENELOPE (solid curve in figure (a)) Monte Carlo codes.

The more detailed picture of physical processes which occur at the e^--beam propagation through the laminated shielding is characterized by the RaT code calculated depth dependencies of the energy flux $\Phi(z)$. They are shown in Fig. 7(b) and can be used to compare the development, in the target, of various radiation components such as primary beam electrons, bremsstrahlung γ-quanta, and the accumulating secondary electrons including δ- and photoelectrons, photon Compton scattering recoil electrons, and those of γ-conversion.

The incident beam electrons mainly contribute to $\Phi(z)$ in the first layers of the target. The $\Phi(z)$ profile is shaped by the competitive effects of their stopping and scattering. The former one augments Φ due to the increase of the electrons path length in a layer. The latter one dumps electron's energy thus reducing Φ. As a result, $\Phi(z)$ is only weakly varying there, *esp.* for $E_e = 2$ and 3 MeV. More in depth z, the stopping becomes dominant, and the primary electrons energy flux drops down by 5÷6 orders of magnitude to the end of the 5$^{\mathrm{th}}$ layer (Cu) at $E_e = 1$ MeV, the end of the 7$^{\mathrm{th}}$ one (Cu) at 2 MeV, and to the target edge at 3 MeV. This corresponds to the decrease in the beam energy down to the lower

energy threshold of the simulation (~10 eV), is fairly consistent with the profiles of Fig. 7(a), and reconfirms the optimal choice of the shield thickness. However, this does not mean the absence of the charged component of radiation behind shielding. The simulation shows that $\Phi(z)$ of secondary electrons is very weakly depth dependent. This is due to their permanent makeup by the bremsstrahlung produced in the target. At the shielding exit, the energy flux of this virtually irremovable component in about $10^{3\div4}$ times higher than that of primary electrons. Finally, in considering the most problematic γ-component of $\Phi(z)$, we see that its production in the frontal, light, layers is more than compensated by its attenuation in the subsequent heavy layers of the laminate. Again, this demonstrates the close to optimal balance of its composition and construction which prevent turning of the electron beam protector to its converter into γ-radiation.

In total, this corollary is illustrated in Fig. 8 which shows the results of the PENELOPE and RaT codes calculations (note, again, their good agreement with each other) of the energy dependence of the conversion factor, the ratio of the total energy of γ-radiation behind shielding and the electron beam energy E_e, in comparison with the simulation data for a tungsten slab of the same thickness t_W = 1.5 mm. One can see that the multilayer structure has the smaller conversion ratio than that of tungsten and, therefore, should be a more efficient shielding when irradiated with electrons.

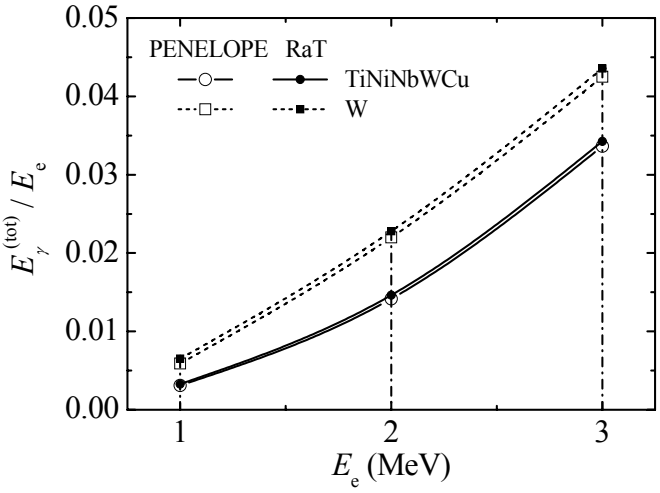

Fig. 8. Electron energy E_e dependencies of the *e*-to-γ energy conversion ratio for 1.5 mm thick laminated composite TiNiNbWCu and tungsten slab of the same thickness. Simulation by means of PENELOPE (open markers) and RaT (closed markers) MC codes.

More reasoned evaluation of the shielding efficiency can be obtained by calculating the absorbed dose *D* in the objects to be protected. This requires either a comprehensive simulation of the target system "shielding + object" or calculations made in some reference conditions. The former task is quite doable but goes beyond the scope of this paper. The latter approach is adopted in the present study. We focus not so much on the magnitudes of dosimetric quantities (which are the radiation source strength and exposure time dependent) but on the comparison of calculation results obtained, under identical conditions, for the TiNiNbWCu laminated shield and for other shielding materials. We chosen to compare with the above studied single-element materials, lightweight aluminum (an electronic protector) and heavy tungsten (a gamma-protector). The correspondent results of calculations are shown in Figs. 9 to 10, and are discussed hereinafter.

Fig. 9 shows the RaT code calculated energy dependences of the photon kerma rate (per one electron of an incident e^--beam) in the air behind shielding. The air-kerma rate $\dot{K}_{air}$, "the total kinetic energy of charged particles released per unit time by indirectly ionizing radiation in the volume of standard air of unit mass" [8], quantifies only the effects owing to the photon component of radiation. It scales with the exposure rate $\dot{X}$, Roentgens per hour, and, in dosimetry, is a conventional measure of the strength of sources of ionizing radiation and the efficiency of biological shielding [1].

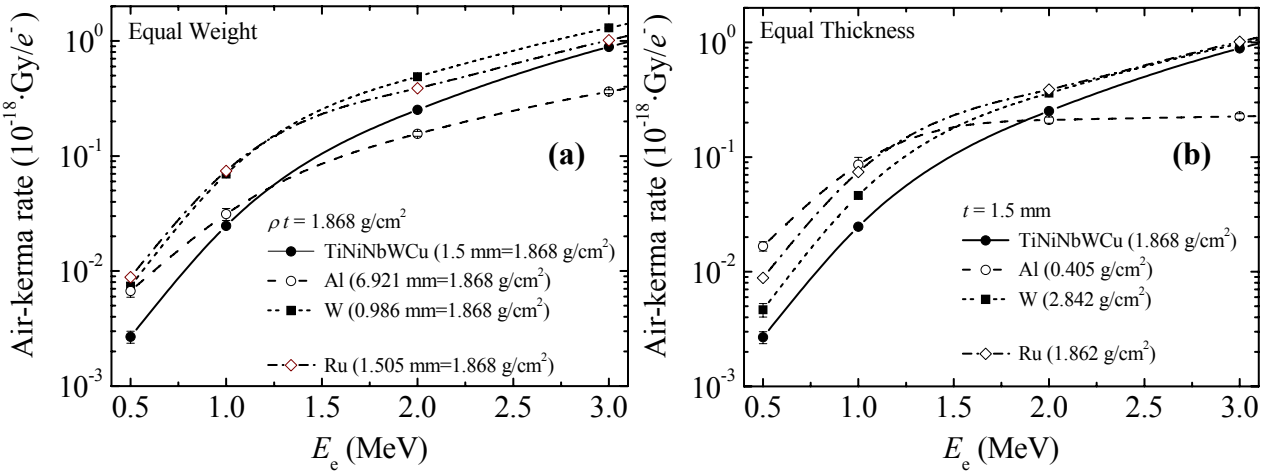

Fig. 9. Electron energy E_e dependencies of the photon air-kerma rate behind the laminated composite TiNiNbWCu shield (●) as compared with the simulation data obtained for Al (○), W (■) and Ru (◇) slabs of the same mass (a) and geometrical (b) thickness.

In Fig. 9(a), the multilayer composite simulation data are compared with those relevant to the weight-equivalent slabs of different shielding materials of the same mass thickness 1.868 g/cm^2. Since the smaller rate means better protection, the laminated composite is much better than tungsten but yields to aluminum in $\dot{K}_{\text{air}}$ at $E_e > 1$ MeV yet surpassing it at lower E_e. The reason is simple. As E_e grows, the thickness of a lightweight Al slab of the same mass is not enough to produce the same magnitude of bremsstrahlung flux the layered shield is first accumulating and then absorbs.

The picture is somewhat different if optimization is not subjected to weight but to dimensions of shielding. The data of Fig. 9(b) show that the multilayer shield outrank both W and Al slabs of the same thickness (1.5 mm). For aluminum, this is evident at $E_e \le 2$ MeV. At higher energies, the photon air-kerma rate comparison is radiation shielding irrelevant since the range R_{Al} exceeds the shield thickness $t_{\text{Al}} = 1.5$ mm starting already from $E_e \approx 800$ keV. Therefore, the 1.5 mm thick Al slab is not suitable for protection against electrons of higher energies where it is just a filter.

Fig. 9 also presents the comparative data for ruthenium (Ru) slabs. Obviously, this rare metal is not used for radiation shielding purposes. Nevertheless, it can be considered as a natural homogeneous analogue of our heterogeneous composite TiNiNbWCu having both an effective atomic number Z_{eff} and an effectively averaged density ρ_{eff} close to the atomic number $Z_{\text{Ru}} = 44$ and the nominal density $\rho_{\text{Ru}} = 12.41$ g/cm^3 of ruthenium, respectively.

The Fig. 9(a,b) data for both Ru slabs of equivalent mass and geometrical thickness illustrate again the essence of the heterogeneity effect on a laminated composite shielding efficiency gain. In Fig. 9, the laminate looks much better than its homogeneous analogue which is clearly far from optimal protection against relativistic electrons of all energies considered. Indeed, despite of its much smaller Z (44 *vs.* 74), ruthenium is almost only as efficient as tungsten.

Since compact and lightweight laminated composites are frequently targeted to the radiation shielding of semiconductor detectors and electronics in aerospace engineering [6,7], we also evaluated, by means of the RaT code simulation, the reference dosimetry quantities valuable for these applications, the rates of Total Ionization Doze (TID) $\dot{D}_{\text{Si}}$ and photon kerma $\dot{K}_{\text{Si}}$ in Silicon (Si, $Z_{\text{Si}} = 14$, $\rho_{\text{Si}} = 2.33$ g/cm^3). The calculation results are shown in Fig. 10.

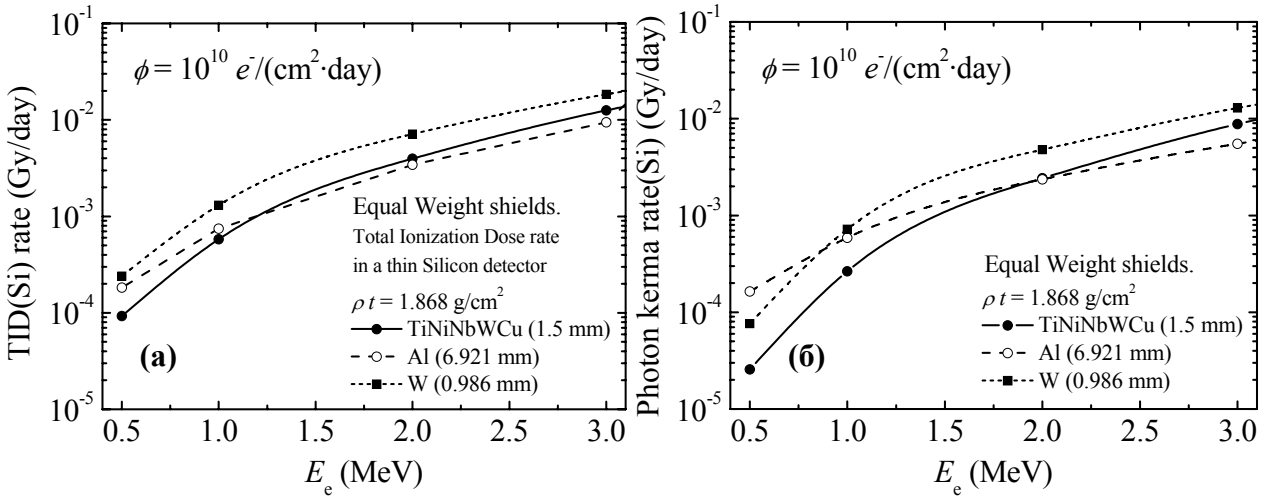

Fig. 10. The electron energy dependencies of the Silicon total ionization dose (a) and photon kerma (b) rates behind the TiNiNbWCu laminated composite shielding (●) compared to those of W (■) and Al (○) slabs of the same mass thickness.

To avoid ambiguities arising from the non-trivial spatial distribution of doses absorbed inside a massive detector, both TID and kerma rates were detected in a negligibly thin (0.1 μm) Si layer located in vacuum immediately behind the shielding. In Fig. 10, the characteristic range of their magnitudes ($\sim 10^{-5} \div 10^{-2}$ Gy per day) corresponds to the characteristic value, $\phi = 10^{10}$ e^-/cm^2 per day, of an electron flux at Low-Earth Orbits (LEO) outside the radiation belts [11].

The Total Ionization Dose (TID) $\dot{D}$ is a key parameter the accumulation of undesired irradiation effects in semiconductors is scaled with. Along with the contribution of the photon component of radiation, the charged components of a shielding outer surface emerged radiation contribute to TID. For this reason, $\dot{D}_{\text{Si}} \ge \dot{K}_{\text{Si}}$ in Fig. 10. This difference is substantial in a Silicon detector surface layer comparable in thickness with the ranges of a shielding emitted secondary electrons but thin as compared with the characteristic MFPs λ of the secondary bremsstrahlung γ-quanta.

For all considered energies of electrons, the comparison of the TiNiNbWCu system TID relevant data of Fig. 10(a) with those of W and Al shields of the same mass per unit area shows that our laminated composite substantially surpasses the tungsten shield and is practically equivalent to that one made of the common material, Al, applied in space.

However, it is worth noting that the aluminum shielding of the same protective efficiency and weight is almost

five times thicker (6.921 mm *vs.* 1.5 mm). Therefore, the developed and vacuum hot rolling solid phase welding fabricated laminated composite shielding has good prospects of application in environments where the simultaneous optimization of radiation shielding by weight, dimensions, and physical and mechanical properties is crucially important.

CONCLUSIONS

This paper presented the consistent procedure of the laminated shielding calculation analysis by means of the Monte Carlo reference code PENELOPE and the original code RaT 3 (NSC KIPT) radiation transport simulation. As against the traditional conservative semi-analytical calculations, its benefits are (i) the detailed reproduction of the radiation shielding design features in the calculation model and (ii) the possibility to obtain the approximation-free and well-founded quantitative results which take into account all the processes of interaction of both primary and internally generated secondary radiations with shielding medium using the up-to-date banks of atomic and nuclear data.

Two interdependent problems were solved within this procedure, (i) a fundamental problem of identification and analysis of physical reasons influencing the shielding efficiency and (ii) an applied problem of calculations of reference dosimetric quantities of transmitted radiation with an adequate view of its complex spectral composition. Our results confirm the potential of this approach by the case of assessment of shielding efficiency of dual and multi-layer composites designed for protection against electrons of moderately relativistic energies, X- and γ-rays.

At detailed simulations of the (e^-,γ)-beams passage through a simple bimetallic dual layer system Al↔W we found an asymmetry of the energy spectrum and dose relevant quantities depending on the order the beam passes through the shielding layers. The "low-to-high-*Z*" ordered shielding Al–W was generally rated as the most efficient one.

We identified the physical reasons of the observed asymmetry. Commonly to both e^--beam and γ-irradiation, it arises only due to secondary radiation (bremsstrahlung, or scattered and fluorescent) produced by a primary beam. Thus, the magnitude of the effect increases with increasing of the layers thicknesses measured, for γ-irradiation, in the mean free path lengths of the photons of characteristic energies, and probably in radiation lengths for the electron incidence.

Other reasons depend on the kind of irradiation and deserve special attention in the photon case. It was shown that the heterogeneity driven asymmetry is maximal for the dual layer Al–W shielding. The shielding efficiency reduces at homogenization or at the increase of the number of Al/W periods. The effect is due to photons Compton scattering in the front lightweight layer (Al) followed by their enhanced absorption in the rear heavy layer (W) or by their backscattering removal. The gain in absorption dominates in thick shields having the attenuation factors $k >> 1$. The γ-albedo enhancement prevails in thin ($k \sim 1$) systems. We also revealed that the asymmetry is strongly spectrally sensitive i.e. an optimal "scatterer↔absorber" arrangement depends on the photon energy. In the upper vicinity of the absorber's photoabsorption edges, the W–Al shielding is more efficient by reason of the resonance fluorescent X-ray yield reduction.

The innovative design of the laminated composite shielding manufactured, in NSC KIPT, by the method of the solid phase vacuum hot rolling joint of layers of materials conforms to all these regularities. The multilayer atomic number shaped structure accounts for both a general trend towards greater efficiency of the "low-to-high-*Z*" grading and a special use of "high-to-low-*Z*" grade to suppress the fluorescence response of the absorber layers.

Its Monte Carlo modeling based design assessment has been accomplished by means of the RaT code radiation transport calculations. Their results were successfully benchmarked against those of the reference code PENELOPE.

This allowed us to quantify, in great detail, the development of radiation cascade in the laminated shielding materials. The detailed picture of the passage, development, and absorption of both electron and bremsstrahlung components in the multilayer shield has been obtained. At last, the calculations of photon air-kerma and Si-absorbed dose rates behind a laminated composite shielding and the comparison with other reference shielding materials (W and Al) have shown that its design is close to optimum for protection against electrons with energies up to 3 MeV when both the shielding weight and dimensions are simultaneously constrained in possible applications.

It can be concluded that the combination of the NSC KIPT advanced techniques of laminated composites manufacturing with the computer-aided prediction, assessment and optimization of their protective efficiency opens up rich possibilities of creating novel radiation protection systems, and is a promising direction for further R&D.

Finally, it is worth noting that the most computationally demandable problem of the laminated composite shielding efficiency optimization still remained beyond the scope of the present paper. To solve it efficiently, it is extremely desired to narrow the extent of Monte Carlo simulations. For this purpose, of great interest is the development and application of the simplified 1D models of different kinds of radiation production and attenuation in the multilayer structures. This went us back to the conventional semi-analytical approach to the shielding dosimetry [1]. The models can make use of certain parameterizations of electrons [23,25] and photons [24] interaction with matter and shall incorporate the operations research techniques (*e.g.*, dynamical programming, or neural networks) for maximization of the shielding efficiency regarding it as a criterion function. The obtained guess design can serve as the reasonable initial problem setup for the subsequent Monte Carlo simulation. The high-precision technique of this paper can be applied to the final design stage for fine optimization of the laminated shielding in view of all fine details of its specific applications.

The authors are grateful to Dr. A.V. Mazilov for providing them with the experimental data used, for comparison, in Fig. 3 of the present paper.

REFERENCES

1. Engineering Compendium on Radiation Shielding, Volume 1: Shielding Fundamentals and Methods / Ed. by R.G. Jaeger. – Berlin, Heidelberg, New York: Springer-Verlag, 1968. – 537 p.
2. Shultis J.K., Faw R.E. Radiation Shielding. – Upper Saddle River, NJ: Prentice Hall PTR, 1996. – 533 p.
3. Stabin M.G. Radiation Protection and Dosimetry: An Introduction to Health Physics. – New York: Springer Science + Business Media, LLC, 2007. – 386 p.
4. Stewart D.Y., Harrison P.F., Morgan B., Ramachers Y. Radiation Shielding for Underground Low-Background Experiments // Nucl. Instr. Meth. – 2007. – Vol. A571, No 3. – P. 651–662. [arXiv:nucl-ex/0607032v1 31 Jul 2006].
5. Singh V.P., Veerendra D.D., Dileep B.N., Sheikh Q., Managanvi S.S., Badiger N.M., Bhat H.R. Background Minimization of HPGe Detector by Passive Graded Shielding // Int. J. of Low Radiation. – 2011. – Vol. 8, No. 4. – P. 313–328.
6. Fan W.C., Drumm C.R., Roeske S.B. Scrivner G.J. Shielding Considerations for Satellite Microelectronics // IEEE Trans. Nucl. Sci. – 1996. – Vol. 43, No. 6. – P. 2790–2796.
7. Spieth B.D., Qassim K.S., Pittman R.N., Russell D.A. Shielding Electronics behind Composite Structures // IEEE Trans. Nucl. Sci. – 1998. – Vol. 45, No. 6, pt. 1. – P. 2752–2757.
8. Greening J.R. Fundamentals of Radiation Dosimetry / 2nd Ed. – New York: Taylor & Francis, 1985. – 190 p.
9. Barnea G., Berger M.J., Seltzer S.M. Optimization Study of Electron-Bremsstrahlung Shielding for Manned Spacecraft // J. Spacecraft Rockets. – 1987. – Vol. 24, No. 2. – P. 158–161.
10. Kesapradist J., Mehlman M. Laminated Lightweight Radiation Shielding Materials. – U.S. Patent EP1120795 A1, Jan. 24, 2000.
11. Stassinopoulos E.G. The Geostationary Radiation Environment // J. Spacecraft Rockets. – 1980. – Vol. 17, No. 2 – P. 145–152.
12. Borts B.V., Vanzha A.F., Lopata A.T., Neklyudov I.M., Shevtchenko S.V. Investigation of Welding Processes of Multilayer Structures Composed from Different Chemical Composition Crystallites by Vacuum Hot Rolling // Problems of Atomic Sci. and Tech.. Ser.: Rad. Damage Phys. and Rad. Mat. Sci. – 2005. – Iss. 5(88). – P. 156–158.
13. Sakcharov V.M. A Method for Estimating the Bremsstrahlung Dose into Spacecraft from Incident Electrons // Radiation Measurements. – 1994. – Vol. 23, No. 1. – P. 53–56.
14. Lazurik V., Lisitskiy A., Pismeneskiy S., Rogov Yu. Effects of Inhomogeneity in Plane Shielding Construction // IEEE Trans. Nucl. Sci. – 2000. – Vol. 47, No. 6. – P. 2132–2134.
15. Metropolis N., Ulam S. The Monte Carlo Method // J. Amer. Stat. Assoc. – 1949. – Vol. 44, No. 247. – P. 335–341.
16. Dyuldya S.V., Bratchenko M.I., Mazilov A.V. On the Asymmetry of Attenuation of Gamma Radiation by Heterogeneous Systems of Compton Scatterers and Absorbers // Abstr. of the 6th Conf. on High Energy Phys., Nucl. Phys. and Accelerators, Feb. 26–29, 2008, Kharkov, Ukraine. – Kharkov: NSC KIPT of NAS of Ukraine, 2008. – P. 109–110.
17. Borts B.V., Bezdverniy P.N., Marchenko I.G. Computer Simulation of the Protective Properties of a Layered Material at Passage of Electrons // Proc. of the 18th Int. Conf. on the Phys. of Rad. Phenomena and Rad. Mat, Sci., Sept. 8–13, 2008, Alushta, Crimea, Ukraine. – Kharkov: "Talent-Trading", 2008. – P. 385–386.
18. Borts B.V., Marchenko I.G., Bezdverniy P.N. Simulation of Electron Transport through the Stratified Composite Material // Problems of Atomic Sci. and Tech. Ser.: Rad. Damage Phys. and Rad. Mat. Sci. – 2009. – Iss. 2(94). – P. 175–177.
19. Baro J., Sempau J., Fernandez-Varea J.M., Salvat F. PENELOPE: An Algorithm for Monte Carlo Simulation of the Penetration and Energy Loss of Electrons and Positrons in Matter // Nucl. Instr. Meth. – 1995. – Vol. B100. – P. 31–46.
20. Salvat F., Fernández-Varea J.M., Acosta E., Sempau J. PENELOPE: A Code System for Monte Carlo Simulation of Electron and Photon Transport // OECD NEA Workshop Proceedings, Nov. 5–7, 2001, Issy-les-Moulineaux, France. – Issy-les-Moulineaux: OECD NEA, 2001. – 234 p.
21. Dyuldya S.V. Computer Experiment in the Physics of Sustainable Technologies of Irradiation Processing of Materials // Bulletin of the V. Karazin Kharkiv National University № 925. Ser.: Mathematical Modeling. Information Technology. Automated Control Systems. – 2010. – Iss. 14. – P. 53–64.
22. Agostinelli S., Allison J., Amako K., Apostolakis J. et al. Geant4 — a Simulation Toolkit // Nucl. Instr. Meth. – 2003. – Vol. A22, No. 3. – P. 250–303.
23. Berger M.J. ESTAR, PSTAR, ASTAR — a PC Package for Calculating Stopping Powers and Ranges of Electrons, Protons and Helium Ions // NIST: Report NISTIR-4999, 1993. (IAEA-NDS-144, IAEA Vienna, Austria, 1993).
24. Boone J.M., Chavez A.E. Comparison of X-ray Cross Sections for Diagnostic and Therapeutic Medical Physics // Med. Phys. – 1996. – Vol. 23, No. 12. – P. 1997–2005.
25. Lazurik V., Tabata T., Lazurik V.T. A Database for Electron-Material Interactions // Rad. Phys. Chem. – 2001. – Vol. 60, No. 3. – P. 161–162.